MNRAS **472,** 2170–2180 (2017)
Advance Access publication 2017 August 17
doi:10.1093/mnras/stx2107

Evolution of the accretion disc around the supermassive black hole of NGC 7213

Jaderson S. Schimoia,[1⋆] Thaisa Storchi-Bergmann,[1] Cláudia Winge,[2] Rodrigo S. Nemmen[3] and Michael Eracleous[4]

[1] *Universidade Federal do Rio Grande do Sul, Astronomy Department, Building 43133 Office M205, Porto Alegre, 90040-060, RS, Brazil*
[2] *Gemini South Observatory, c/o AURA Inc., Casilla 603, La Serena, Chile*
[3] *Departamento de Astronomia, Instituto de Astronomia, Geofísica e Ciências Atmosféricas, Universidade de São Paulo, São Paulo, SP 05508-090, Brazil*
[4] *Department of Astronomy and Astrophysics and Institute for Gravitation and the Cosmos, Pennsylvania State University, 525 Davey Lab, University Park, PA 16802, USA*

Accepted 2017 August 11. Received 2017 August 11; in original form 2016 December 26

ABSTRACT

We present observations of the double-peaked broad H α profile emitted by the active nucleus of NGC 7213 using the Gemini South Telescope in 13 epochs between 2011 September 27 and 2013 July 23. This is the first time that the double-peaked line profile of this nucleus – typical of gas emission from the outer parts of an accretion disc surrounding a supermassive black hole (SMBH) – is reported to vary. From the analysis of the line profiles we find two variability time-scales: (1) the shortest one, between 7 and 28 d, is consistent with the light travel time between the ionizing source and the part of the disc emitting the line; and (2) a longer one of $\gtrsim$3 m corresponding to variations in the relative intensity of the blue and red sides of the profile, which can be identified with the dynamical time-scale of this outer part of the accretion disc. We modelled the line profiles as due to emission from a region between $\approx$300 and 3000 gravitational radii of a relativistic, Keplerian accretion disc surrounding the SMBH. Superposed on the disc emissivity, the model includes an asymmetric feature in the shape of a spiral arm with a rotation period of $\approx$21 m, which reproduces the variations in the relative intensity of the blue and red sides of the profile. Besides these variations, the rms variation profile reveals the presence of another variable component in the broad line, with smaller velocity width W_{68} (the width of the profile corresponding to 68 per cent of the flux) of $\sim$2100 km s^{-1}.

Key words: accretion, accretion discs – line: profiles – galaxies: individual (NGC 7213) – galaxies: nuclei – galaxies: Seyfert.

1 INTRODUCTION

NGC 7213 is a nearby ($z = 0.005839$) Sa spiral galaxy. Its active nucleus was first classified as Seyfert 1 by Phillips (1979) based on its very broad H α emission line (13 000 km s^{-1} for the full width at zero intensity) and later was also recognized as low-ionization nuclear emission-line region (LINER) by Filippenko & Halpern (1984) based on a study of a variety of optical emission lines which were observed to have full width at half-maximum (FWHM) in the range of 200–2000 km s^{-1}. Its nucleus harbours a $\sim 10^8$ M$_\odot$ supermassive black hole (SMBH, Woo & Urry 2002), producing a bolometric luminosity of $L_{\rm bol} = 7 \times 10^{43}$ erg s^{-1} (Emmanoulopoulos et al. 2012).

The nucleus of NGC 7213 has been extensively studied in X-rays. *XMM–Newton*/*BeppoSAX* observations revealed that the active galactic nucleus (AGN) spectrum shows no significant Compton reflection component (Bianchi et al. 2003) – what is very peculiar amongst bright Seyfert 1 AGNs. Additionally, these observations also revealed the presence of a significant Fe K complex. Bianchi et al. (2008) reported the data analysis of a long *Chandra* High Energy Transmission Grating observation finding that the neutral iron K α line has a FWHM of 2400^{+1100}_{-600} km s^{-1}, claiming that it was fully consistent with the H α FWHM (2640^{+1100}_{-600} km s^{-1}). This seems to be at odds with the previous studies that showed a much broader profile or it may indicate a strong variation of the profile. Bianchi et al. (2008) concluded that the neutral Fe K line originates in the Compton-thin broad-line region (BLR) to explain the absence of Compton reflection and of any relativistic component in the lines. More recently, Lobban et al. (2010) reproduced the highly ionized

⋆ E-mail: silva.schimoia@ufrgs.br

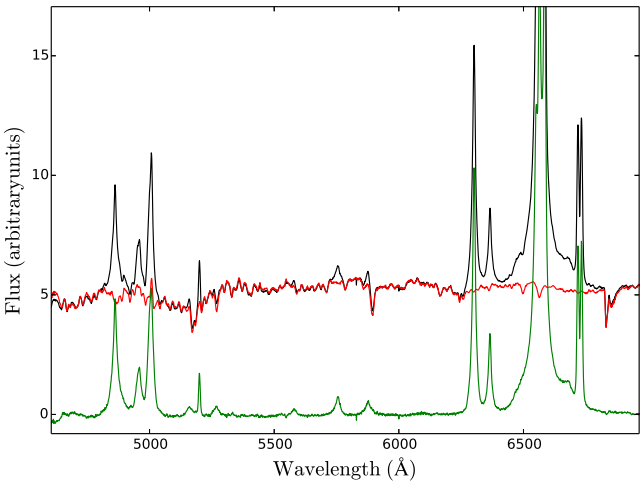

Figure 1. Example of the process of stellar population subtraction for the spectrum obtained in 2012 July 21. Top: the black solid line is the nuclear spectrum extracted within a window of 1.0 arcsec × 1.0 arcsec; the red solid line is the stellar population template obtained by averaging two extranuclear spectra at 2.0 arcsec from the nucleus, scaled to match the continuum of the nuclear extraction. Bottom: the green solid line is the resulting *nuclear emission spectrum*, after subtracting the stellar population template.

iron K lines with a photoionization model where gas has a column density of $N_H > 10^{23}$ cm^{-3} and is likely to be located between 10^3–10^4 gravitational radii (R_g) from the central source. The authors suggest that the inner accretion flow is radiatively inefficient (Radiatively Inefficient Accretion Flow, e.g. Yuan & Narayan 2014), which would explain the photoionization spectrum and the absence of the optically thick disc component.

Although the broad Hα emission line of NGC 7213 has been reported in previous works (Phillips 1979; Filippenko & Halpern 1984; Storchi-Bergmann et al. 1996), there are no variability studies of its profile to date. A recent study by Schnorr-Müller et al. (2014) (see Fig. 1) showed its Hα line to present a very broad double-peaked component. Very broad double-peaked lines – with velocity separation of ∼10 000 km s^{-1} between the blue and red peaks are thought to originate in the outer parts of an accretion disc (Schimoia et al. 2012; Lewis, Eracleous & Storchi-Bergmann 2010). Models of ionized gas rotating in a relativistic Keplerian accretion disc around a SMBH have been successful in accounting for such double-peaked profiles (Chen, Halpern & Filippenko 1989; Chen & Halpern 1989; Storchi-Bergmann et al. 2003; Strateva et al. 2003; Lewis et al. 2010). These models explain most of the observed features of the profiles (Eracleous & Halpern 2003) and can help to constrain the physical properties of the line emitting part of the disc, as, for instance, the inner and outer limits for the emitting region as well as its inclination relative to the plane of the sky. Although other models have been considered for the origin of the double-peaked profiles, these are much less attractive than the accretion disc model (see discussion in Eracleous & Halpern 2003; Eracleous, Lewis & Flohic 2009)

Double-peaked profiles are expected to vary. Lewis et al. (2010) and Gezari, Halpern & Eracleous (2007) studied such variation for 14 double-peaked emitters in a long-term monitoring of these sources at time intervals ranging from several months to years. They found that all profiles showed variability on time-scales of years. Recently, Schimoia et al. (2012, 2015), monitored the double-peaked Hα profile of NGC 1097 on shorter time-scales and found that, besides presenting variations on similarly long (1.5 yr) time-scales, the profile also varied on time-scales as short as a week or even shorter. They concluded that there are different time-scales of variability in this source, which should apply also to other double-peak emitters, including NGC 7213.

In this paper we model, for the first time, the double-peaked Hα profile of the NGC 7213 nucleus as due to emission from the outer parts of a relativistic, Keplerian accretion disc, constraining its properties. We also present a study of its variation from spectral monitoring of the profile over a time span of almost two years, from 2011 September 27 to 2013 July 23, including one time interval as short as a week. We find that the variation of the profiles reveal that, not only the double-peaked profile varies, on short and long time-scales, but there is another broad component, with a velocity width ∼2100 km s^{-1}, that is also variable.

This paper is organized as follows: in Section 2 we describe the observations and the data reduction; in Section 3 we present the observational results, the adopted accretion disc model, and the discovery of an additional variable component to the profile; in Section 4 we discuss the time-scales of the accretion disc variability, the interpretation and implications of the modelling to the structure of the AGN and explore a determination of the mass of the SMBH through the model; and the conclusions of this work are presented in Section 5.

2 OBSERVATIONS AND DATA REDUCTION

We obtained a total of 13 optical spectra of the nucleus of the galaxy NGC 7213 from 2011 September 27 to 2013 July 23. The observation of 2011 September 27 was obtained with the Integral Field Unit of the Gemini Multi Object Spectrograph (GMOS-IFU) at the Gemini South telescope (Schnorr-Müller et al. 2014, Gemini project GS-2011B-Q-23). These observations consisted of two adjacent IFU fields (covering 7 arcsec × 5 arcsec each) resulting in a total angular coverage of 7 arcsec × 10 arcsec around the nucleus. The wavelength range of this observation was 5600–7000 Å in order to cover Hα+[N II] λλ6548,6583 and [S II] λλ6716,6731 observed with the grating R400-G5325, which resulted in a resolution of R ≈ 2000 (∼150 km s^{-1}). The seeing during the IFU observations was 0.5 arcsec, what results in a spatial resolution of 58 pc, and the sampling of the final reduced cube is 0.1 arcsec × 0.1 arcsec.

The remaining 12 observations were taken between 2012 July 21 and 2013 July 23 with the spectrograph GMOS of the Gemini South telescope in the longslit mode (project ID GS-2012A-Q-86). The slit used was 1.0 arcsec wide and 330 arcsec long and was oriented at the position angle of 305° in all observations. The grating was B600-G5323 with the central wavelength of 5700 Å chosen to cover the Hα+[N II] λλ6548,6583 and Hβ 4862 Å and give a spectral resolution of R ≈ 1688 (∼177 km s^{-1}). The instrumental setup of the longslit observations resulted in a pixel scale of 0.14 arcsec pixel^{-1}. Most visits consisted of six exposures each, giving a total of 2700 s on source. Table 1 lists the dates of the observations, the instruments, number and length of exposures on each visit. The data were reduced using the standard procedures and packages for IFU and longslit modes in IRAF.[1] Throughout the paper, in all figures, the spectra are shown at the rest wavelength.

[1] IRAF is distributed by the National Optical Astronomy Observatories, which are operated by the Association of Universities for Research in Astronomy, Inc., under cooperative agreement with the National Science Foundation.

Table 1. Observations of NGC 7213.

UT date	MJD	Mode	Exposures
2011 September 27	55831.130	IFU	12 × 350
2012 July 21	56129.155	Longslit	6 × 450
2012 July 30	56138.422	Longslit	6 × 450
2012 October 15	56215.111	Longslit	6 × 450
2012 November 22	56253.047	Longslit	6 × 450
2013 April 13	56395.383	Longslit	6 × 450
2013 May 11	56423.386	Longslit	6 × 450
2013 May 20	56432.315	Longslit	6 × 450
2013 May 30	56442.334	Longslit	6 × 450
2013 June 14	56457.399	Longslit	6 × 450
2013 June 30	56473.310	Longslit	6 × 450
2013 July 07	56480.218	Longslit	6 × 450
2013 July 23	56496.278	Longslit	6 × 450

Note. Column (1) gives the date of observations while column (2) gives the Modified Julian Date (JD−2400000.5). Column (3) is the mode of observation and column (4) gives the number of visits and the exposure time of each visit.

2.1 Subtraction of the underlying stellar population contribution

We extracted the nuclear spectra from our data using a window of 1.0 arcsec × 1.0 arcsec centred on the peak of the continuum emission. Within this aperture, the continuum is dominated by the underlying stellar population. In order to isolate the AGN emission we subtracted the contribution of the stellar population. The process is illustrated in Fig. 1, and is described as follows:

(i) First we extracted the nuclear spectrum.

(ii) Two extranuclear spectra, also within windows of 1.0 arcsec × 1.0 arcsec, were extracted at 2.0 arcsec away from both sides of the nucleus.

(iii) The two extranuclear spectra were averaged. The average spectrum was scaled to match the flux of the continuum of the nuclear spectrum, as it displays the same absorption features with the same equivalent widths to those of the nuclear spectrum. This indicates that the nuclear spectrum shows no detectable non-stellar continuum emission, only line emission (as in our previous studies of NGC 1097 Storchi-Bergmann et al. 2003; Schimoia et al. 2015). The average extranuclear spectrum is only weakly 'contaminated' by narrow emission lines which were excised by using a synthetic spectrum obtained from the application of the STARLIGHT-V04 spectral synthesis code of Cid Fernandes et al. (2005).

(iv) The scaled and corrected stellar population template was then subtracted from the nuclear spectrum in order to isolate the AGN emission.

After the subtraction of the stellar population template we adopted the spectrum of 2011 September 27 (MJD 55831) – which has the best signal-to-noise ratio (12 × 350 s of exposure on the source) – as the reference spectrum, and calibrated the other spectra by scaling the flux of the narrow lines [O I]6300 Å and [O I]6363 Å to match those of the reference spectrum. The [O I] lines are thought to originate in a larger region than that producing the broad double-peaked Balmer lines, thus these [O I] lines should not display significant variations in their flux during the time span of the observations, these lines are also isolated and unaffected by broad, variable emission lines. After this 'intercalibration' by the [O I] emission lines we measured the flux of the narrow [S II] λλ6716, 6731 lines in the different spectra finding small variations of 7–8 per cent in the line fluxes. We thus conclude that the flux calibration amongst the spectra leads to uncertainties of 7–8 per cent in the line fluxes. This uncertainty was added in quadrature to the other uncertainties in our measurements.

3 RESULTS

The resulting nuclear emission spectra, after subtraction of the underlying stellar population and calibration by the narrow emission lines, are shown in Fig. 2. This figure shows that in the first observation of 2011 September 27 the blue and red peaks were very prominent in the H α profile, with the blue peak higher than the red peak. During the second observation of 2012 July 21 (MJD 56129), taken almost 10 months after the first, the profile shows less pronounced peaks, mainly the blue peak, whose flux decreased to the point of becoming lower than the red peak. The red side of the profile is now more prominent than the blue side. The overall flux of the double-peaked profile decreased from 2011 September 27 to 2012 July 21, thus showing that the time interval of 10 months between these two observations is large enough to allow significant changes in the shape and flux of broad H α double-peaked profile.

After this long time interval between the first two observations, we monitored the profile more frequently in order to look for shorter variability time-scales. We found such variations. For instance, from 2012 July 30 (MJD 56138) to 2012 October 15 (MJD 56215), the profile changed showing mainly a decrease in flux in the red wing. In the subsequent spectra the profile continued to change, with the overall flux always lower than that of the first observation. While in the first observation one can clearly see a blue and a red peak in the profile, in most of the other observations the shape of the profile can be better described as showing a double shoulder instead of double peak.

3.1 Measurements of the flux variations of the broad double-peaked emission line

In order to measure the flux of the double-peaked line and quantify its variations, we proceeded as follows:

(i) We first removed the contribution of the narrow emission lines interpolating a linear effective continuum between ∼6513 Å and ∼6648 Å excising the emission lines H α+[N II]λλ6548,6583 above this continuum. We performed the same process between ∼6703 Å and ∼6751 Å to remove the [S II] λλ6716,6731 emission lines. The removed emission lines are shown as grey regions in Fig. 3.

(ii) After the removal of the narrow emission lines we defined two parameters: $F_{\rm Blue}$ which is the integrated flux under the blue side of the broad double-peaked profile, between 6395 Å and 6563 Å and $F_{\rm Red}$ which is the integrated flux under the red side of the double-peaked profile, between 6563 Å and 6820 Å. Since we have corrected the spectra by the redshift, the definition of 6563 Å as the wavelength that divides the fluxes of the blue and red sides is equivalent to use as reference the systemic velocity of the galaxy, as 6563 Å is the rest wavelength of H α.

$F_{\rm Blue}$ is illustrated as the blue region in Fig. 3, while $F_{\rm Red}$ is the red region in the same figure. We note that our definition is such that the wavelength range covered by the red side is wider than that of the blue side of the profile. This effect is expected due to (at least partially) the gravitational redshift, since the high velocity wings of the profile come from gas that is very close to the SMBH (∼300 gravitational radius; see following discussion on the modelling of the profile).

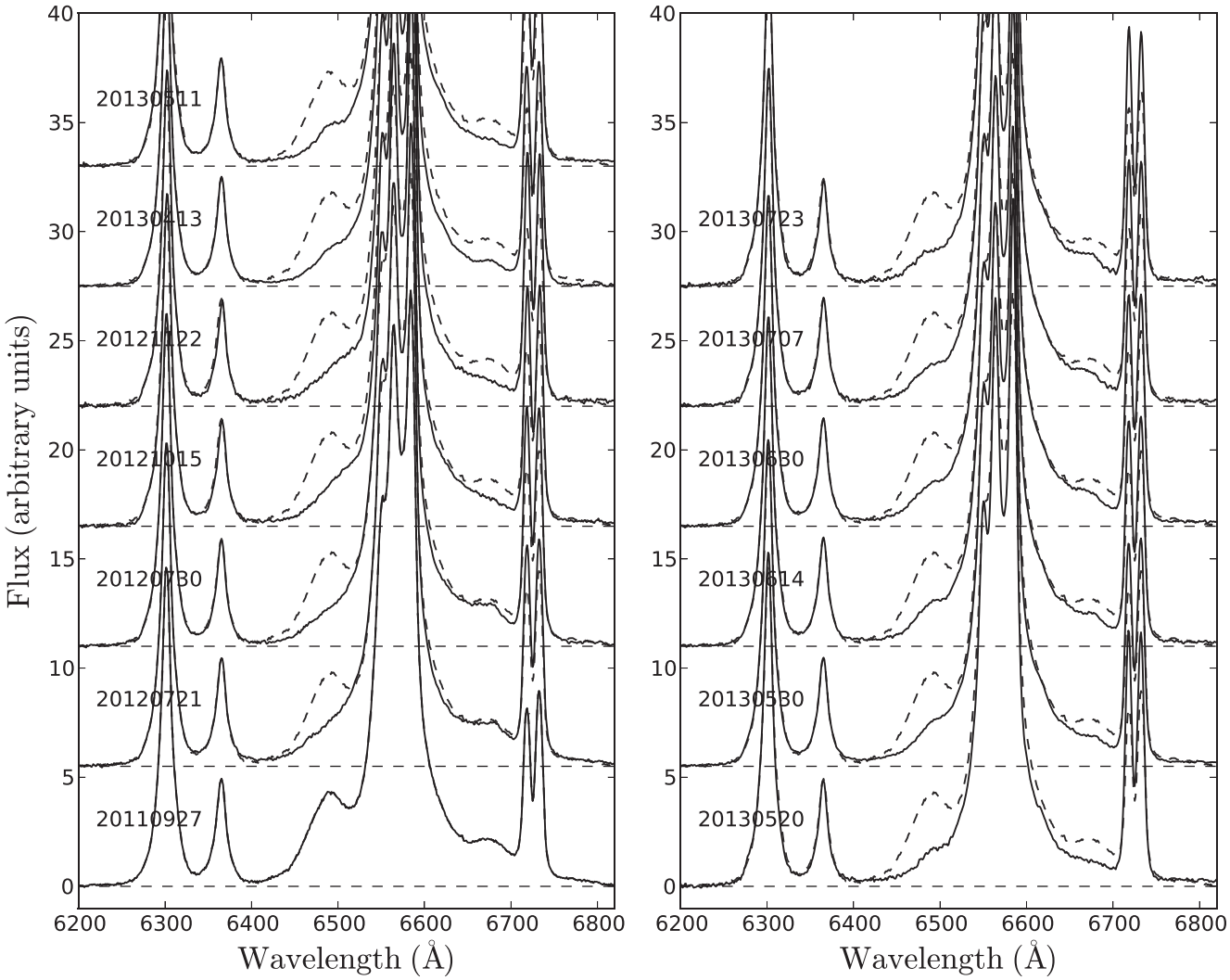

Figure 2. The nuclear emission line profiles from 2011 September 27 (MJD 55831) to 2013 July 23 (MJD 56496). The reference spectrum of 2011 September 27 (MJD 55831) is displayed in each panel in dashed lines for comparison.

(iii) $F_{\rm DP}$ was then obtained as the sum of $F_{\rm Blue}$ and $F_{\rm Red}$ (being thus the total integrated flux of the double-peaked line), while $F_{\rm Red}/F_{\rm blue}$ was obtained from the ratio between $F_{\rm Blue}$ and $F_{\rm Red}$.

The parameters defined above are similar to those used to quantify the variability of the double-peaked profile of NGC 1097 (Schimoia et al. 2015). The main difference is that the double-peaked profile of NGC 7213, in some epochs, does not display clear blue and red peaks, but shoulders, instead. Thus, instead of measuring the flux density and position of the blue and red peaks we rather measured the integrated flux of each side of the double-peaked line, which is more robust for this case. The values of $F_{\rm Blue}$, $F_{\rm Red}$, $F_{\rm DP}$ and $F_{\rm Red}/F_{\rm blue}$ are listed in Table 2, while the time variation of these parameters is shown in Fig. 4.

3.2 Variability time-scales

From our previous studies of the broad double-peaked H α profile of NGC 1097, we concluded that it shows two main variability time-scales: a long one, identified as a dynamical time-scale for the gas orbiting in the disc (see Section 4); and a shorter one that can be identified with the light travel time between the ionizing source and the emitting portion of the disc. In NGC 7213, we tentatively identify these time-scales as follows:

(i) *Long variability time-scale*: significant changes in the integrated flux of the double-peaked profile can occur on time-scales of a few months. For instance, from 2012 July 21 (MJD 56129) to 2012 November 22 (MJD 56253) $F_{\rm DP}$ decreased by $\sim$30 per cent in approximately four months. During the same period, the relative intensity of the red and blue sides of the profile, $F_{\rm Red}/F_{\rm blue}$, also changed by 46 per cent. But we also note that between 2013 April 13 (MJD 56395) and 2013 July 23 (MJD 56496) – a time interval of $\sim$100 d – $F_{\rm Red}/F_{\rm blue}$ almost did not vary, keeping a value of $\sim$1.5. We thus conclude that the time-scale of the $F_{\rm Red}/F_{\rm blue}$ variations is $\gtrsim$3 m.

(ii) *Short variability time-scale*: from 2013 April 13 to 2013 July 23 we obtained more frequent observations, separated by time intervals of a week to a month. The shortest time interval between consecutive observations is 7 d (from 2013 June 30 to 2013 July 07). On this time-scale $F_{\rm DP}$ did not display changes larger than the uncertainties in the measurements. During the period from 2013 April 13 (MJD 56395) to 2013 May 11 (MJD 56423) $F_{\rm DP}$ changed from 409.8 $\pm$ 22.1 to 461.6 $\pm$ 25 $\times$ 10^{-15} erg s^{-1} cm^{-2} thus by

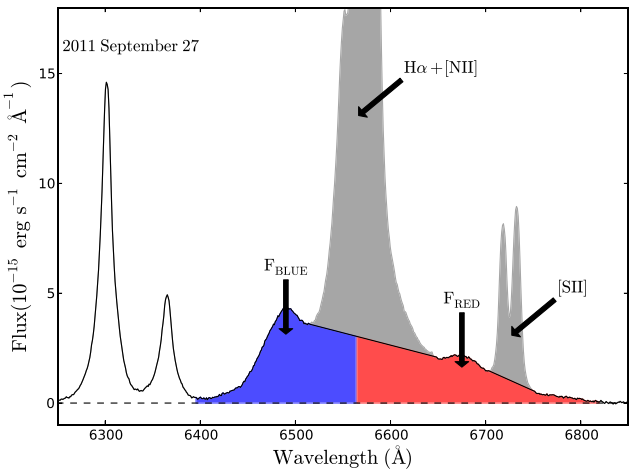

Figure 3. The measured characteristics of the broad double-peaked H α profile $F_{\rm Blue}$ and $F_{\rm Red}$. The grey regions are emission lines that were removed before measuring the flux of the double-peaked profile. The blue region, between 6395 Å and 6563 Å shows the area integrated to obtain the flux of the blue side of the profile, $F_{\rm Blue}$. The red region, between 6563 Å and 6820 Å , shows the same for the red side of the profile, $F_{\rm Red}$.

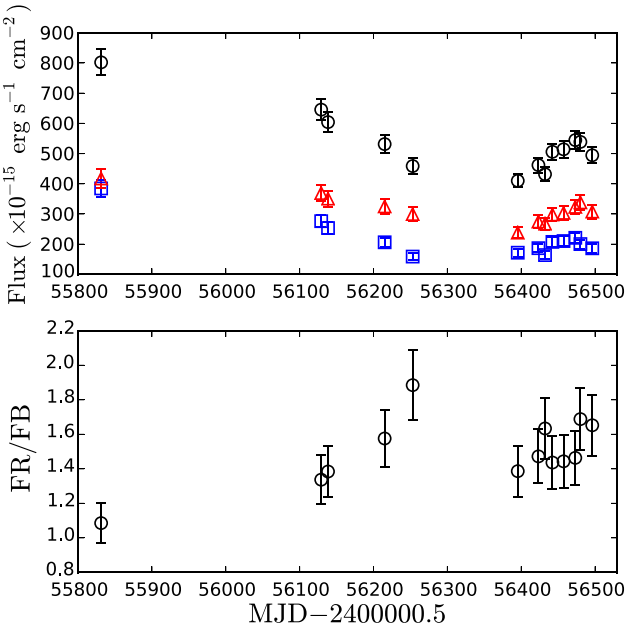

Figure 4. Top panel: the black circles represent the integrated flux of the broad double-peaked line, $F_{\rm DP}$. The blue squares represent the integrated flux of the blue side of the line – $F_{\rm Blue}$, while the red triangles represent the integrated flux of the red side of the line – $F_{\rm Red}$. All measurements were performed after excising the narrow emission lines as illustrated in Fig. 3. Bottom panel: the black circles represent the temporal evolution of $F_{\rm Red}/F_{\rm blue}$– the ratio between $F_{\rm Red}$ and $F_{\rm Blue}$.

10 per cent in a time interval of 28 d. We can thus only put limits on the shortest time-scale: it is probably longer than a week but shorter than 28 d. We note that this week-to-28 d for the shortest time-scale of variability was obtained for our specific set of observations. Since we did not sample the profile in a time interval shorter than 7 d, we may have missed possible stochastic variations that may have occurred on a shorter time-scale.

3.3 The rms spectrum

Fig. 2 shows that the broad double-peaked profile clearly varies with time. Variations in the illumination of the disc and/or the presence of structures eventually developing in the disc can explain these variations. In order to investigate which regions of the profile show more variations, we have calculated the root mean square (rms) spectrum – $F_{\rm rms}(\lambda)$ – which can reveal if there are specific regions in the velocity space in which the flux varies more. The rms spectrum, $F_{\rm rms}(\lambda)$, is calculated as the rms variation of the flux at each wavelength covered by the double-peaked profile. As discussed in Section 3.1, significant changes in $F_{\rm DP}$ and in the shape of the double-peaked profile are only seen on time-scales $\gtrsim$30 d. Thus, in order to calculate the rms spectrum, we selected spectra that are separated by time intervals of the order of 30 d, namely: 2011 September 27, 2012 July 21, 2012 October 15, 2012 November 22, 2013 April 13, 2013 May 20, 2013 June 14, 2013 July 07.

The resulting rms spectrum is shown in Fig. 5. The largest variations in the profile are observed in three 'peaks': two of them

Table 2. NGC 7213 double-peaked line measurements

UT date	MJD	$F_{\rm Blue}$	$F_{\rm Red}$	$F_{\rm DP}$	$F_{\rm Red}/F_{\rm blue}$
2011 September 27	55831.130	384 ± 29	417 ± 31	802 ± 43	1.1 ± 0.1
2012 July 21	56129.155	276 ± 21	369 ± 28	646 ± 35	1.3 ± 0.1
2012 July 30	56138.422	253 ± 19	351 ± 26	604 ± 33	1.4 ± 0.2
2012 October 15	56215.111	206 ± 16	325 ± 24	532 ± 29	1.6 ± 0.2
2012 November 22	56253.047	159 ± 12	300 ± 23	458 ± 26	1.9 ± 0.2
2013 April 13	56395.383	173 ± 13	238 ± 18	410 ± 22	1.4 ± 0.2
2013 May 11	56423.386	187 ± 14	275 ± 21	462 ± 25	1.5 ± 0.2
2013 May 20	56432.315	164 ± 12	268 ± 20	432 ± 24	1.6 ± 0.2
2013 May 30	56442.334	208 ± 16	298 ± 22	506 ± 27	1.4 ± 0.2
2013 June 14	56457.399	210 ± 16	304 ± 23	514 ± 28	1.5 ± 0.2
2013 June 30	56473.310	221 ± 17	324 ± 24	545 ± 29	1.5 ± 0.2
2013 July 07	56480.218	200 ± 15	338 ± 25	539 ± 30	1.7 ± 0.2
2013 July 23	56496.278	187 ± 14	308 ± 23	495 ± 27	1.7 ± 0.2

Note. Column (1) gives the date of observations while column (2) gives the Modified Julian Date (JD−2400000.5). Column (3) gives the integrated flux of the blue side of the double-peaked line in units of 10^{-15} erg s^{-1} cm^{-2} and the column (4) gives the integrated flux of the red side of the line in the same units. Column (5) gives total flux of the double-peaked line. Column (6) gives the ratio between (4) and (3).

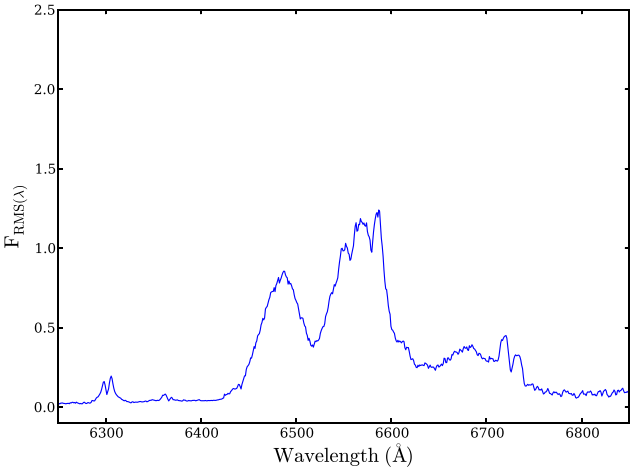

Figure 5. The rms spectrum calculated from our data. The blue and red humps are observed at the wavelengths of the two peaks of the double-peaked profile, but the central hump shows the presence of another component showing similar variation to that of the double-peaked component. Some residuals, of the order of the uncertainties in the cross-calibration of the spectra, are observed at the wavelengths of the narrow emission lines.

coinciding in wavelength with the blue and red peaks of the double-peaked profile and a third peak observed in between the two peaks, centred at a velocity close to zero (adopted as the velocity of the narrow Hα component). The double-peaked structure is expected for variable emission in an accretion disc, but the central hump reveals that there is significant variation also in a lower velocity structure, resembling another broad component with a velocity width of $\approx$2100 km s^{-1} (see discussion below). Some residual variation is also observed at the wavelengths of the narrow lines, but this is due to the estimated uncertainties of the 'intercalibration' of the data, as discussed previously.

The blue and red peaks of the rms spectrum support the origin of the double-peaked emission and its variability, from gas emission in an accretion disc with variable surface emissivity. We will thus model such emission with an Keplerian relativistic accretion disc in the next sections. But, besides the double-peaked component, there are also comparable flux variations at lower projected velocities, indicating the presence of another varying component besides the one attributed to the accretion disc. This component could be due to emitting clouds orbiting the SMBH at distances beyond the outer border of the disc, as it shows much smaller FWHM than that of the double-peaked line. We will call this component 'central-broad component', or CBC, for short. In our modelling, described in the next sections, we will take into account the contribution of this component via the fit of three Gaussian components to it.

3.4 The Accretion Disc Model

We modelled the double-peaked Hα profiles using the accretion disc model described by Gilbert et al. (1999), Storchi-Bergmann et al. (2003) and Schimoia et al. (2012, 2015). In this formulation, the broad double-peaked emission line originates in a relativistic Keplerian disc of gas surrounding the SMBH. The line-emitting portion of the disc is circular and located between an inner radius ξ_1 and an outer radius ξ_2 – where ξ is the disc radius in units of the gravitational radius $r_g = GM_\bullet/c^2$, c is the speed of light, G is the gravitational constant and $M_\bullet$ is the mass of the black hole. The disc has an inclination angle i with respect to the plane of the sky.

In order to take into account the observed asymmetries on the double-peaked profile we adopted the 'saturated spiral model' (Schimoia et al. 2012) for the total emissivity of the accretion disc. In this formulation, there is an enhancement of the emissivity in the form of a spiral arm, which is superposed on the underlying emissivity of the circular accretion disc. The details of the emissivity law are described in Storchi-Bergmann et al. (2003) and Schimoia et al. (2012). Here we briefly describe the physical meaning of the different parameters which are relevant for our modelling.

The parameter ξ_q is the radius of the maximum emissivity, or saturation radius, at which the emissivity law changes; q_1 is the index of the emissivity law for $\xi_1 < \xi < \xi_q$; q_2 is the index for $\xi_q < \xi < \xi_2$. The presence of the spiral arm enhances the emissivity of the gas where it is located, thus the parameter A represents the brightness contrast between the emissivities of the spiral arm and the underlying disc. The emissivity of the spiral arm decays as a function of the azimuthal distance $\phi - \psi_0$ from the ridge line to both sides of the arm, assumed to be a Gaussian with an azimuthal width of δ. Furthermore, ϕ_0 is the azimuthal angle of the spiral pattern, p is the pitch angle and ξ_{sp} is the innermost radius of the spiral arm (cf. Schimoia et al. (2015) for more details).

We kept the emissivity index for radii larger than the break radius as $q_2 = 3$, as proposed by Dumont & Collin-Souffrin (1990), after the saturation radius the emissivity of the disc is expected to be proportional to ξ^{-3}. We tested many values for the emissivity index for the region between the inner and the saturation radius, $\xi_1 < \xi < \xi_q$, and concluded that $q_1 = -0.2$ gave the best fits; this small value for q_1 is required because, as can be seen in Fig. 2, the broad double-peaked profile displays very extended wings. The presence of extended wings means that the inner parts, with higher projected velocities, are important for the emissivity of the disc and the value $q_1 = -0.2$ implies that the emissivity increases slowly until the break radius, which makes the inner parts of the accretion disc important with respect to the outer parts. We also tested different values for the inner and outer radii, ξ_1 and ξ_2, and the inclination angle, i, and found that the set of values that best reproduced all the data together are $\xi_1 = 300 \pm 60$, $\xi_2 = 3000 \pm 90$ and $i = 47^\circ \pm 2^\circ$, so in the analysis below, we keep these values for these parameters.

In order to reproduce the double-peaked profile variations, namely, in the relative intensity of the blue and red sides of the double-peaked profile and the broadening/narrowing of the profile, we first modelled the reference spectrum (with the best signal-to-noise ratio), from 2011 September 27; and after finding the best parameter values for this epoch, we allowed only three parameters to vary: ϕ_0, A and ξ_q. The parameters that define the shape of the spiral arm were kept fixed at $p = 13^\circ$, $\delta = 75^\circ$ and $\xi_{sp} = \xi_1$. Amongst these parameters, the pitch angle is the less uncertain because it regulates the curling of the spiral arm, and in the case of NGC 7213, a small pitch angle ($p = 13^\circ$) is required to curl the spiral arm close to the inner radius and give relative more importance to the inner regions of the disc, and consequently, better reproduce the wings of the profile. Fig. 6 shows the best fit for each epoch while the corresponding parameters are listed in Table 3. Surface emissivity maps corresponding to the models are shown in Fig. 7.

3.5 The central broad component (CBC)

Fig. 6 shows that the accretion disc model can reproduce the broad double-peaked emission line in our observations, and we thus confirm that its emission originates from gas rotating in a relativistic Keplerian disc with very high projected velocities (e.g. $\sim$ 8550 km s^{-1}

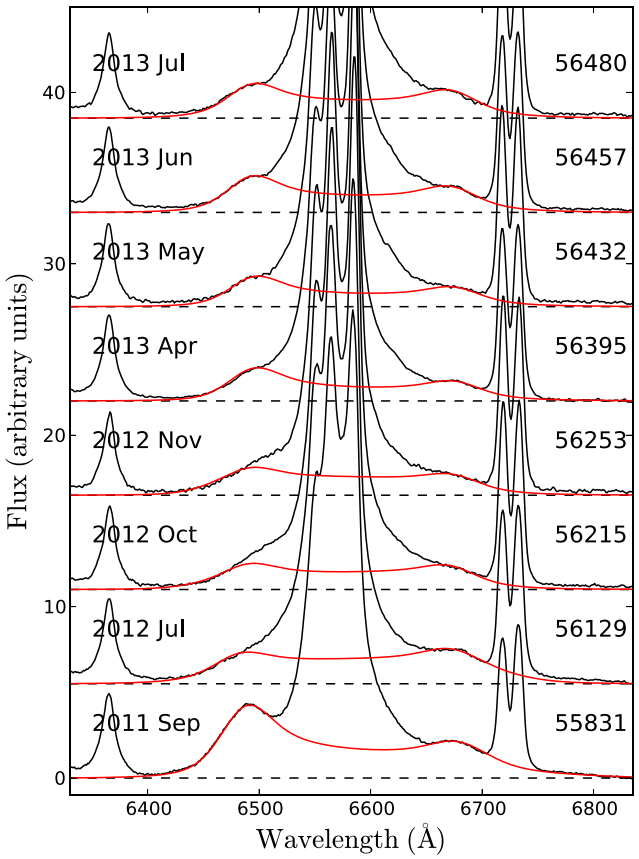

Figure 6. The black solid line is the profile observed in different epochs, after subtraction of the stellar continuum and calibration by the flux of the narrow lines. In each frame the red solid line represents the emission of the accretion disc model that best fits the double-peaked profile. The spectra are shifted in flux for better visualization. The parameters of each fit are listed in Table 3.

Table 3. NGC 7213 best-fittings parameters of the accretion disc model.

UT date	MJD	ξ_q	A	$\phi_0(^\circ)$
2011 September 27	55831.130	1800	4.0	+280
2012 July 21	56129.155	2000	3.0	+205
2012 October 15	56215.111	2500	2.0	+45
2012 November 22	56253.047	2500	3.0	+25
2013 April 13	56395.383	2500	2.0	−30
2013 May 20	56432.386	2500	1.8	−50
2013 June 14	56457.399	3000	1.0	−60
2013 July 07	56480.218	3000	0.2	−80

Note. Column (1) gives the date of observations while column (2) gives the Modified Julian Date (JD−2400000.5). Column (3) gives the break or saturation radius ξ_q, column (4) gives the contrast of the spiral arm A and column (5) gives the orientation of the spiral arm ϕ_0 as it rotates in the disc.

is the velocity separation between the blue and red peaks of the double-peaked profile of 2011 September 27).

But the rms spectrum of Fig. 5 shows that besides the broad double-peaked component there is another varying component that appears as an excess variation above that attributed to the gas that is rotating in the accretion disc, observed at lower project velocities. We have called this component CBC. The CBC is not easily seen in the profile because of the blended narrow emission lines H α+[N II] that sit 'on top' of it. It cannot be due to the narrow lines because the

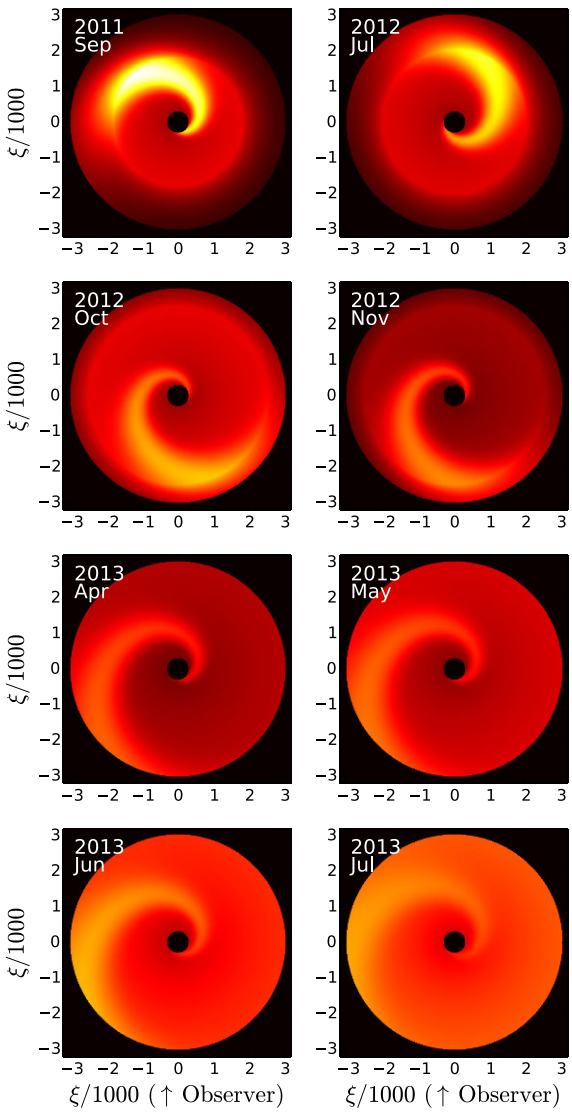

Figure 7. Emissivity maps corresponding to the accretion disc models fitted to the double-peaked profiles of Fig. 6. The yellow to white represents regions with the highest surface emissivity, while the dark red represents the regions with the lowest surface emissivity. The non-axisymmetric part of the emissivity has the shape of a spiral arm rotating in the accretion disc. The observer sees the disc from the bottom of the figure and the spiral arm rotates clockwise. The epoch of observation is written in the top left corner of each frame.

observed variation is larger than the estimated 8 per cent variations attributed to the uncertainties in the intercalibration using the narrow lines.

We inspected the IFU data in order to check if the CBC and the broad double-peaked line were detectable outside the nucleus, considering our spatial resolution of 58 pc. We did not find evidence for the presence of the CBC neither the double-peaked line beyond this 58 pc region, concluding that both of them are unresolved, consistent with an origin in the outer parts of the accretion disc or in the BLR.

In order to measure the contribution of the CBC in each epoch and characterize its profile, it is necessary to separate the CBC from the narrow lines. We have used the following method to do this:

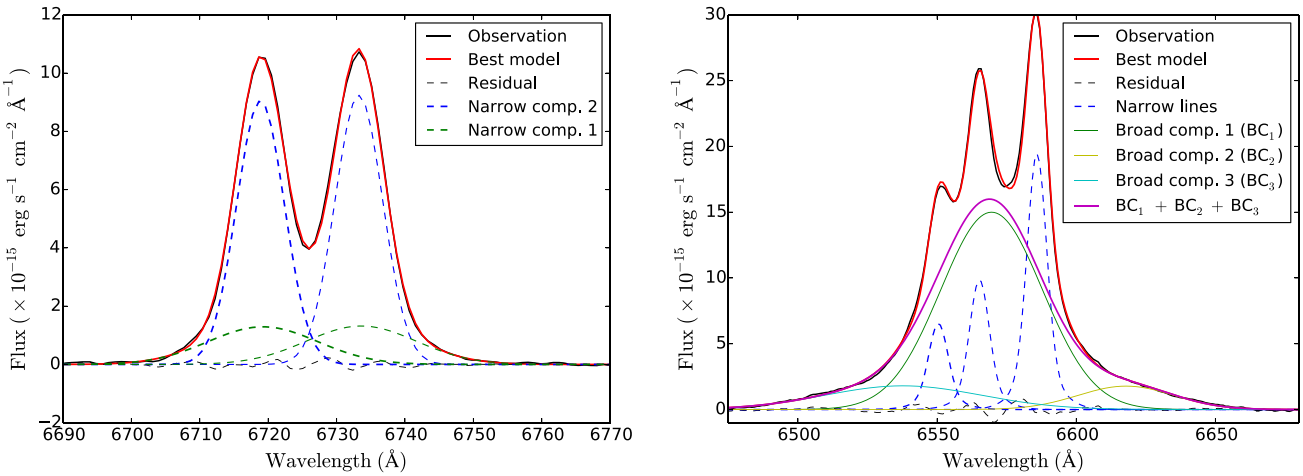

Figure 8. Left: fit of the narrow emission lines [S II] λλ6716, 6731. Each narrow line was fitted using two Gaussian components which are represented by the blue and green dashed lines. The central velocity and velocity width of each component was constrained to be the same for both [S II] lines. The red solid line is the best fit to the lines and represents the sum of the individual components, and the black dashed line is the residual from the fit. Right: fit of the H α CBC and narrow components of H α+[N II] λλ6548, 6583. The narrow components were constrained to have the same velocities as the [S II] lines. The fitted components to the narrow lines are shown as dashed blue lines. The CBC was fitted with three Gaussian components; the sum of the three is shown as a continuous magenta line and the individual components are shown in green, yellow and cyan. The solid red line is the sum of all components and the residual (observed – modelled) is shown as a black dashed line.

(i) We first subtracted the modelled double-peaked profile from each spectrum, and then fitted the narrow emission lines [S II] λλ6716, 6731. These lines were fitted with two Gaussian components each, as the use of only one Gaussian did not fit well the base of the lines. Each Gaussian component was constrained in velocity space to have the same central velocity and width in the two lines of the [S II] doublet. An example of the fit to the [S II] lines is shown in the left-hand panel of Fig. 8. The broader of the two narrow components of [S II] λλ6716, 6731 has typical central velocity of 66 ± 17 km s^{-1} and velocity dispersion of 329 ± 17 km s^{-1}; the other narrow component has central velocity and velocity dispersion of 41 ± 8 and 159 ± 5 km s^{-1}, respectively.

(ii) Since the narrow emission line components of H α+[N II] λλ6548, 6583 are superposed on the H α CBC that we want to characterize, in order to decrease the degeneracy in the fit, we adopted the physically motivated assumption that these components originate in the same region as the [S II] lines, thus fixing the centroid velocities and widths of the Gaussians to the corresponding values of the [S II] lines. The flux of the lines was allowed to vary, only constraining the flux of [N II] λ6583 to be 2.87 times the flux of [N II] λ6548 (Osterbrock & Ferland 2006).

(iii) Once we constrained the centre and dispersion velocities of the H α+[N II] narrow components, (and the flux constraints above) we fitted the H α CBC together with these lines. For the fit of the CBC we used three Gaussian components. An illustration of the result of this fit is shown in the right-hand panel of Fig. 8. The magenta line represents our fit for the CBC, whose flux accounts for a significant part of the total broad H α line (comprising the contributions of the double-peaked component plus the CBC).

After fitting the broad double-peaked H α, the narrow emission lines H α+[N II]λλ6548,83 and the CBC, we calculated the *mean*, *rms* and *minimum* spectra from our 8 modelled observations, as well as of the modelled profiles.

The top pannel of Fig. 9 shows the mean spectrum we have calculated from our data. This spectrum displays double-shoulders,

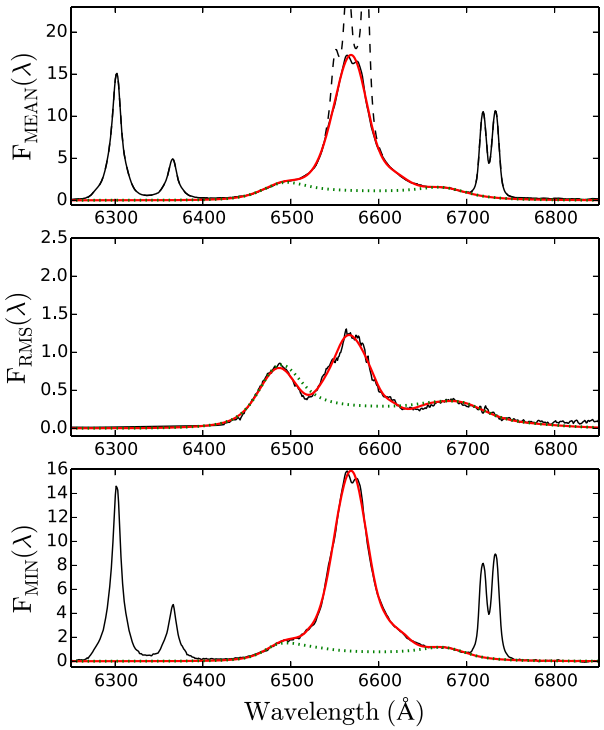

Figure 9. Top: the black dashed line is the mean spectrum calculated from our observations, while the solid black line is the mean spectrum calculated after subtracting the contribution of the H α+[N II] λλ6548, 6583 narrow lines. The green dotted line is the mean model spectrum of the accretion disc. The solid red line is the mean spectrum of the total broad H α emission calculated from the accretion disc models + the fitted CBC. Middle: the rms variations of the observed and modelled spectra. Bottom: the minimum observed and modelled spectra.

with the maximum flux density of the blue side of the profile slightly higher than that of the red side, which is well modelled by our mean accretion disc model, shown as the green dotted line. In addition we note that the CBC H α component also contributes strongly to the mean overall broad H α emission.

Before calculating the rms spectrum we subtracted the contribution of the narrow emission lines, and the result is shown in the middle pannel of Fig. 9. The rms spectrum, for both the data and the models (red line) shows that, as discussed before, the most variable portion of the spectrum shows a profile with three peaks: a blue peak centred around 6487 Å, a red peak centred around 6684 Å, in agreement with the expected variations in the accretion disc plus a central peak corresponding to variations in the CBC. The similarity between the black (observations) and red (model) profiles shows that the variations in the broad profile can be well reproduced by the rms profile of our accretion disc model (green dotted line) plus the CBC (modelled via the fit of three Gaussinas to each profile).

The minimum spectrum was constructed by selecting, at each wavelength, the minimum flux from all spectra. This minimum spectrum represents a base profile which is common to all profiles, and is shown at the bottom panel of Fig. 9. In the scenario in which the emission arises from a circular accretion disc with an emissivity enhancement (such as a spiral arm, as we have considered in our modelling), the minimum spectrum would be that of the underlying accretion disc. Fig. 9 shows that the minimum spectrum also displays two shoulders, consistent with the above assumption. Individually or taken together, the mean, rms and minimum spectra all support the scenario where the origin of the broad, double-peaked line profile is indeed a rotating disc. The CBC is evidence of additional gas at lower line-of-sight velocities than the gas in the accretion disc, probably orbiting the SMBH at distances beyond the disc.

3.5.1 *Properties of the CBC*

We have measured three properties of the CBC: the integrated flux, $F_{\rm CBC}$; the peak velocity, $V_{\rm peak}$, which is the velocity corresponding to the wavelength of maximum flux and the median velocity; V_{50}, which corresponds to the wavelength at which the integrated flux under the profile corresponds to 50 per cent of the total flux. As the profile is not fitted by only one Gaussian and contains asymmetries, we adopted as velocity dispersion the velocities above and below the median velocity that encompass 34 per cent of the flux under the profile, $\pm\sigma_V$. We list these measurements in Table 4.

We note that the CBC flux $F_{\rm CBC}$, is usually $\sim$50–100 per cent higher than the flux of the double-peaked component, $F_{\rm DP}$ (the only exception being the first epoch). However, during the campaign, the amplitude of the variations of the $F_{\rm CBC}$ was lower than that of the $F_{\rm DP}$: while $F_{\rm DP}$ varied between minimum and maximum fluxes of 410 and 802 $\times$ 10^{-15} erg s^{-1} cm^{-2}, respectively, $F_{\rm CBC}$ varied between minimum and maximum fluxes of 803 and 921 $\times$ 10^{-15} erg s^{-1} cm^{-2}, respectively. This behaviour is also evident from a comparison of the top and middle panels of Fig. 9: the CBC is much more pronounced in the mean spectrum than in the rms spectrum. We define a proxy for the velocity width of the CBC as

$$W_{68} = +\sigma_V - (-\sigma_V), \quad (1)$$

which represents the velocity width of the line that contains 68 per cent of the total line flux around V_{50}. The values of W_{68} are listed in the last column of Table 4. The average value of the parameter W_{68} is 2100 $\pm$ 73 km s^{-1}, which represents the average velocity width of the CBC.

Table 4. NGC 7213 CBC properties.

UT date	MJD	$F_{\rm CBC}$	$V_{\rm peak}$	$V_{50} \pm \sigma_V$	W_{68}
2011 September 27	55831.130	921 $\pm$ 74	253	274^{+1046}_{-920}	1966
2012 July 21	56129.155	936 $\pm$ 75	211	148^{+1004}_{-1045}	2049
2012 October 15	56215.111	891 $\pm$ 71	253	274^{+1088}_{-1087}	2175
2012 November 22	56253.047	803 $\pm$ 64	253	274^{+1046}_{-1003}	2049
2013 April 13	56395.383	829 $\pm$ 66	253	274^{+1046}_{-1003}	2049
2013 May 20	56432.315	831 $\pm$ 67	253	274^{+1130}_{-1003}	2133
2013 June 14	56457.399	889 $\pm$ 71	253	274^{+1171}_{-1003}	2174
2013 July 07	56480.218	904 $\pm$ 72	253	274^{+1171}_{-1003}	2174

Note. Column (1): date of observations; column (2): Modified Julian Date (JD−2400000.5); column (3): integrated flux of the CBC in units of 10^{-15} erg s^{-1} cm^{-2} and the uncertainties are $\pm$8 per cent of the measured flux; column (4): peak velocity of the line; column (5): median velocity of the line plus/minus the velocities corresponding to $\pm$34 per cent of the integrated flux; column (6): velocity width of the CBC that contains 68 per cent of the total line flux around V_{50}. Velocity units are in km s^{-1}.

4 DISCUSSION

4.1 Low-state of the double-peaked profile

Differently from what was observed by Schimoia et al. (2015) for the *low state* of the double-peaked profile of NGC 1097, when NGC 7213 is in a low state it is hard to detect the asymmetry in the broad profile. This means that, when the $F_{\rm DP}$ flux is low, the contrast between the spiral arm and the underlying disc fades. This fading can be observed in the emissivity maps of Fig. 7. In the first epoch the contrast parameter was A = 4.0, but in the last it was very small: A = 0.2. Between 2013 April 13 (MJD 5639) and 2013 July 23 (MJD 56496), the overall flux $F_{\rm DP}$ stayed low (did not show much variation), and the ratio $F_{\rm Red}/F_{\rm blue}$ stayed almost the same, around 1.5. This result is in agreement with the decrease in the contrast between the arm and the underlying disc during the last observations.

4.2 Implications for the mass of the SMBH

The epoch that most clearly shows the blue and red peaks in the double-peaked profile is 2011 September 27. In this profile we measure a velocity separation between the blue and red peaks of $\Delta v \approx 8850$ km s^{-1}. Considering half of this velocity as a characteristic velocity for the gas in the disc, corresponding approximately to the radius of maximum emission, and correcting this value for the inclination of the disc, we obtain a circular velocity $V_{\rm C} = \frac{8850}{2} \times \frac{1}{\sin(47^\circ)} \sim 6050$ km s^{-1}.

As discussed in Section 3, the shortest variability time-scale in $F_{\rm DP}$ probably lies between 7–28 d. If we adopt 17 – the middle between these two limits – as the light-travel time between the central ionizing source (that we adopt as approximately coinciding with the location of the SMBH) and the radius of maximum emission, we can estimate the mass of the SMBH as $M_\bullet = 1.21 \times 10^8$ M$_\odot$. Considering that this radius could be in the range between the lower and upper limits of 7 and 28 d, respectively, the resulting range for the SMBH mass estimate is $5 \times 10^7 < M_\bullet < 2 \times 10^8$ M$_\odot$.

An independent estimate of the mass of the SMBH can be obtained via the $M_\bullet - \sigma_\star$ relation of Tremaine et al. (2002):

$$\log\left(\frac{M_\bullet}{\mathrm{M}_\odot}\right) = \alpha + \beta \log\left(\frac{\sigma_\star}{\sigma_0}\right), \quad (2)$$

where $\alpha = 8.13 \pm 0.06$; $\beta = 4.02 \pm 0.32$; and $\sigma_0 = 200\,\mathrm{km\,s^{-1}}$. The scatter in the $M_\bullet - \sigma_\star$ relation is not included in the error, but the error bars on the coefficients are.

When we performed the stellar population synthesis with STARLIGHT-V04, we used the simple stellar population templates of Bruzual & Charlot (2003) and allowed the fit of the stellar kinematics. The value we obtained for the velocity dispersion was $\sigma = 219\,\mathrm{km\,s^{-1}}$. We have corrected this value for the instrumental resolution, σ_{inst}, and the resolution of the template spectra, σ_{base}, as follows:

$$\sigma_\star^2 = \sigma^2 - \sigma_{\mathrm{inst}}^2 + \sigma_{\mathrm{base}}^2. \quad (3)$$

The B600 grating that we used in the longslit GMOS observations has an instrumental resolution of $\sigma_{\mathrm{inst}} = 177\,\mathrm{km\,s^{-1}}$, while the Bruzual & Charlot (2003) base of simple stellar population spectra has a resolution of $R = 2000$, thus $\sigma_{\mathrm{base}} = 150\,\mathrm{km\,s^{-1}}$, in the wavelength range 3200–9500 Å. We thus obtain a stellar velocity dispersion of $\sigma_\star = 198\,\mathrm{km\,s^{-1}}$, which via equation (2) gives $M_\bullet = 1.29 \times 10^8\,\mathrm{M}_\odot$, in very good agreement with the value we have obtained via the estimated light travel time between the nuclear ionizing source and the radius of maximum emission of the line emitting disc.

This value that we have obtained for the stellar velocity dispersion is also very close to the value $\sigma_\star = 185\,\mathrm{km\,s^{-1}}$ previously obtained by Woo & Urry (2002), who also used the $M_\bullet - \sigma_\star$ relation (Tremaine et al. 2002) to estimate the mass of the SMBH as $M_\bullet = 9.77 \times 10^7\,\mathrm{M}_\odot$. Considering that there is an intrinsic scatter of ∼0.3 dex (a factor ∼2) in the $M_\bullet - \sigma_\star$ relation, we conclude that both our determinations of the mass of the SMBH are in good agreement with this previous determination, supporting this value.

4.3 Variability time-scales

The two shortest variability time-scales of standard accretion discs are the *light travel time-scale*, τ_1, and the *dynamical time-scale*, τ_{dyn} (Frank, King & Raine 2002):

$$\tau_1 = 6 M_8 \xi_3\ \mathrm{d} \quad (4)$$

$$\tau_{\mathrm{dyn}} = 6 M_8 {\xi_3}^{3/2}\ \mathrm{m}, \quad (5)$$

where M_8 is the mass of the SMBH in units of $10^8\,\mathrm{M}_\odot$ and $\xi_3 = \xi \times 10^{-3}$. Adopting the mass of the SMBH in NGC 7213 as $M_\bullet = 1.29 \times 10^8\,\mathrm{M}_\odot$ and considering the best model inner and outer radius of the accretion disc, $0.3 < \xi_3 < 3$, we obtain a range for the variability time-scales of

(i) τ_1: 2.3 – 23 d
(ii) τ_{dyn}: 1.3 – 40 m

The evolution of the model parameter ϕ_0 – the azimuthal angle of the spiral pattern, with time is shown in Fig. 10. A linear fit to the data gives an angular velocity of $\alpha \approx -0.^\circ58\,\mathrm{d^{-1}}$, which implies a rotation period of ∼620 d or 21 m, within the expected range of the dynamical time-scale above. Considering this period of rotation as a dynamical time-scale of the accretion disc, it suggests that the asymmetric feature of the accretion disc has completed almost one full rotation. The observed precession period of the spiral pattern is also in good agreement with the theoretical predictions for m = 1 modes in massive, Keplerian discs by Adams, Ruden & Shu (1989) and Shu et al. (1990).

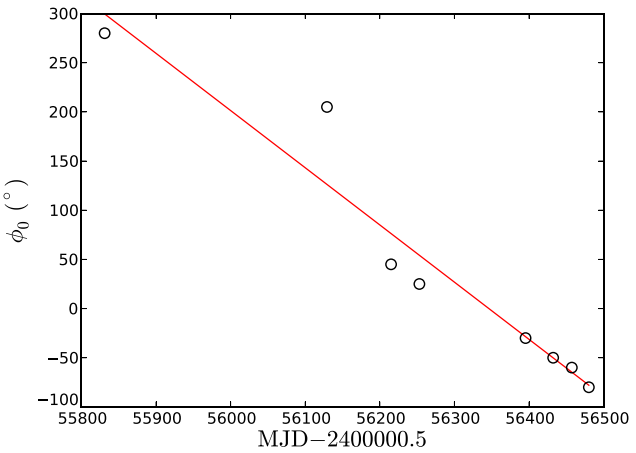

Figure 10. The black open circles represent the parameter ϕ_0 for each modelled epoch. The red solid line is the best linear fit to the data, which has an angular coefficient of $\alpha \approx -0.^\circ58\,\mathrm{d^{-1}}$. The rotation period corresponds to $P \approx 620$ d or 21 m.

From Fig. 4, it can be further concluded that variations in the relative intensity of fluxes of the red and blue sides of the profile, $F_{\mathrm{Red}}/F_{\mathrm{blue}}$, occur in the time-scale of a few months. For instance: $F_{\mathrm{Red}}/F_{\mathrm{blue}}$ varied from 1.09 (2011 September 27) to 1.33 (2012 July 21) in almost 10 months and also varied from 1.33 (2012 July 21) to 1.67 (2012 November 22) in approximately four months. This variation is also within the range of the dynamical time-scale, and compatible with the rotation period of the spiral arm in the accretion disc discussed above.

Regarding the shortest variability time-scale, although our relatively sparse monitoring did not allow us to put strong constraints on its value, the range we have estimated, between 7 and 28 d is approximately consistent with the light travel time.

4.4 The CBC

The mean velocity width of the CBC, $\overline{\mathrm{W}_{68}} = 2100 \pm 73\,\mathrm{km\,s^{-1}}$ suggests it is located at larger distances from the SMBH than the disc. Estimating its variability time-scale from the line flux – considering typical uncertainties of ∼8 per cent – we obtain ∼120 d, ∼6 times the outer radius of the disc. The central velocity of the CBC of $\mathrm{V}_{50} = 260 \pm 40\,\mathrm{km\,s^{-1}}$ is much larger than the gravitational redshift at the above distance, that suggests the presence of a bulk motion of this region.

The presence of a CBC together with disc-like profiles have been also found by other authors, e.g. Ho et al. (1997) and Storchi-Bergmann et al. (2017). Their methodology for subtracting the contribution of the narrow lines and fitting the broad central component is very similar to the methodology adopted in the present work. These authors found mean values of the FWHM for the broad component of $\sim 2000\,\mathrm{km\,s^{-1}}$ (Ho et al. 1997) and $\sim 1500 \pm 500$ (Storchi-Bergmann et al. 2016), which are consistent with the value of $\overline{\mathrm{W}_{68}} = 2100 \pm 73\,\mathrm{km\,s^{-1}}$ we found for NGC 7213.

5 CONCLUSIONS

We have presented 13 new optical spectra of the broad Hα profile of the AGN in NGC 7213 over a time span of 22 months, with

observations sparsed by time intervals from a week to a few months. The main results of this paper are given below.

(i) It is the first time that variability is reported for the broad ($\approx$8550 km s^{-1} for the velocity separation of the blue and red peaks) Hα line of this AGN, that shows a double-peaked profile, typical of gas rotating in an accretion disc around a SMBH.

(ii) The relative intensity of the integrated flux of the blue and red sides of the double-peaked profile displayed significant variations on a time-scale $\gtrsim$3 mo, consistent with the *dynamical time-scale* of gas rotating in an accretion disc around a 10^8 M$_\odot$ SMBH.

(iii) The total flux of the broad line showed variations on a time-scale between 7 and 28 d, consistent with the *light travel time-scale* between the ionizing source and the emitting part of the disc.

(iv) The rms variation spectrum reveals that the most variable part of the broad Hα line shows three peaks: a blue and a red peak consistent with an origin in the accretion disc plus an additional central peak which we attribute to a CBC, showing similar amplitude to those of the two other peaks.

(v) We successfully modelled the broad double-peaked profile as due to gas emission from a region of a Keplerian and relativistic accretion disc with inner and outer radii of $\xi_1 = 300 \pm 60$ and $\xi_2 = 3000 \pm 90$ (in units of gravitational radii), respectively, and inclination angle of $i = 47^\circ \pm 2^\circ$ relative to the plane of the sky. We also found that the disc harbours a spiral arm with varying contrast relative to the underlying disc.

(vi) The variations in the relative intensity of the blue and red sides of the profile were modelled as due the rotation of the spiral arm, with a period of $\sim$21 m. This arm completed almost one full rotation in the accretion disc and faded (decreased its contrast) over the approximately two years spanned by the observations.

(vii) The profile of the CBC was modelled via the fit of three Gaussians; it shows an average width velocity (proxy for the velocity dispersion) of $W_{68} = 2100 \pm 73$ km s^{-1}, which suggests that the gas of this component is located at larger distances from the SMBH than the outer radius of the disc.

(viii) Using the fit of the stellar absorption features with the STARLIGHT-V04 code we obtained a velocity dispersion of the bulge of $\sigma_\star = 188$ km s^{-1}, what implies a mass for the SMBH of $M_\bullet = 1.29 \times 10^8$ M$_\odot$ via the $M_\bullet - \sigma_\star$ relation, in agreement with previous determinations.

(ix) We also estimated the mass of the SMBH using a representative velocity of the gas in the disc and the light travel time between the SMBH and the disc. We find that the SMBH mass is in the range $5 \times 10^7 < M_\bullet < 2 \times 10^8$ M$_\odot$, also in agreement with the previous and our above estimate.

In summary, our proposed scenario for the origin of the broad Hα profile of NGC 7213 is the following: the broad double-peaked emission arises from a Keplerian and relativistic accretion disc, inclined by 47 degrees relative to the plane of the sky from a region with inner and outer radii of $\approx$300 and 3000 gravitational radii, respectively. This disc orbits a SMBH with a mass in the range $5 \times 10^7 \leq M_\bullet \leq 2 \times 10^8$ M$_\odot$. The relative intensity of the flux of blue and red sides of the double-peaked profile changes due to the rotation of a spiral arm with a rotation period of 21 months. The contrast between the arm and underlying disc decreased gradually during approximately two years of observations, leading to ever smaller asymmetries between the heights of the blue and red sides of the double-peaked profile. An additional component, the CBC, also contributes to the variable broad Hα profile as a central 'hump' observed at velocities close to systemic, with a velocity width of 2100 km s^{-1}. We propose that this component originates in gas that is also orbiting the black hole but is either at larger radii in the accretion disc or not coplanar with the disc.

ACKNOWLEDGEMENTS

JSS acknowledges CNPq, National Council for Scientific and Technological Development – Brazil. RN acknowledges support from FAPESP.

REFERENCES

Adams F. C., Ruden S. P., Shu F. H., 1989, ApJ, 347, 959
Bianchi S., Matt G., Balestra I., Perola G. C., 2003, A&A, 407, L21
Bianchi S., La Franca F., Matt G., Guainazzi M., Jimenez Bailón E., Longinotti A. L., Nicastro F., Pentericci L., 2008, MNRAS, 389, L52
Bruzual G., Charlot S., 2003, MNRAS, 344, 1000
Chen K., Halpern J. P., 1989, ApJ, 344, 115
Chen K., Halpern J. P., Filippenko A. V., 1989, ApJ, 339, 742
Cid Fernandes R., Mateus A., Sodré L., Stasińska G., Gomes J. M., 2005, MNRAS, 358, 363
Dumont A. M., Collin-Souffrin S., 1990, A&A, 229, 313
Emmanoulopoulos D., Papadakis I. E., McHardy I. M., Arévalo P., Calvelo D. E., Uttley P., 2012, MNRAS, 424, 1327
Eracleous M., Halpern J. P., 2003, ApJ, 599, 886
Eracleous M., Lewis K. T., Flohic H. M. L. G., 2009, New Astr. Rev. 53, 133
Filippenko A. V., Halpern J. P., 1984, ApJ, 285, 458
Frank J., King A., Raine D. J., 2002, Accretion Power in Astrophysics, 3rd edn. Cambridge Univ. Press, Cambridge, p. 398
Gezari S., Halpern J. P., Eracleous M., 2007, ApJS, 169, 167
Gilbert A. M., Eracleous M., Filippenko A. V., Halpern J. P., 1999, in Gaskell C. M., Brandt W. N., Dietrich M., Dultzin-Hacyan D., Eracleous M., ASP Conf. Ser. Vol. 175, Structure and Kinematics of Quasar Broad Line Regions. Astron. Soc. Pac., San Francisco, p. 189
Ho L. C., Filippenko A. V., Sargent W. L. W., Peng C. Y., 1997, ApJS, 112, 391
Lewis K. T., Eracleous M., Storchi-Bergmann T., 2010, ApJS, 187, 416
Lobban A. P., Reeves J. N., Porquet D., Braito V., Markowitz A., Miller L., Turner T. J., 2010, MNRAS, 408, 551
Osterbrock D. E., Ferland G. J., 2006, in Osterbrock D. E., Ferland G. J., Astrophysics of Gaseous Nebulae and Active Galactic Nuclei. University Science Books, Mill Valley, CA
Phillips M. M., 1979, ApJ, 227, L121
Schimoia J. S., Storchi-Bergmann T., Nemmen R. S., Winge C., Eracleous M., 2012, ApJ, 748, 145
Schimoia J. S., Storchi-Bergmann T., Grupe D., Eracleous M., Peterson B. M., Baldwin J. A., Nemmen R. S., Winge C., 2015, ApJ, 800, 63
Schnorr-Müller A., Storchi-Bergmann T., Nagar N. M., Ferrari F., 2014, MNRAS, 438, 3322
Shu F. H., Tremaine S., Adams F. C., Ruden S. P., 1990, ApJ, 358, 495
Storchi-Bergmann T., Rodriguez-Ardila A., Schmitt H. R., Wilson A. S., Baldwin J. A., 1996, ApJ, 472, 83
Storchi-Bergmann T. et al., 2003, ApJ, 598, 956
Storchi-Bergmann T., Schimoia J. S., Peterson B. M., Elvis M., Denney K. D., Eracleous M., Nemmen da Silva R., 2017, ApJ, 835, 236
Strateva I. V. et al., 2003, AJ, 126, 1720
Tremaine S. et al., 2002, ApJ, 574, 740
Woo J.-H., Urry C. M., 2002, ApJ, 579, 530
Yuan F., Narayan R., 2014, ARA&A, 52, 529

This paper has been typeset from a TEX/LATEX file prepared by the author.